Pergamon

Int. J. Solids Structures Vol. 34, No. 26, pp. 3355–3371, 1997
Published by Elsevier Science Ltd
Printed in Great Britain
0020-7683/97 $17.00 + .00

PII: S0020-7683(96)00215-6

GENERALIZED FINITE ELEMENT FORMULATION FOR SMART MULTILAYERED THERMAL PIEZOELECTRIC COMPOSITE PLATES

HO-JUN LEE
National Aeronautics and Space Administration, Lewis Research Center, 21000 Brookpark Road, Mail Stop 23-3, Cleveland, Ohio 44135-3191, U.S.A.

and

DIMITRIS. A. SARAVANOS†
Ohio Aerospace Institute, Brook Park, Ohio 44142, U.S.A.

(*Received* 30 *April* 1996; *in revised form* 11 *October* 1996)

Abstract—Analytical formulations are presented which account for the coupled mechanical, electrical, and thermal response of piezoelectric composite laminates and plate structures. A robust layerwise theory is formulated with the inherent capability to explicitly model the active and sensory response of piezoelectric composite plates having general laminations in thermal environments. Finite element equations are derived and implemented for a bilinear 4-noded plate element. Applications demonstrate the capability to manage thermally induced bending and twisting deformations in symmetric and antisymmetric composite plates with piezoelectric actuators and attain thermal stability. The resultant stresses in the thermal piezoelectric composite laminates are also investigated. Published by Elsevier Science Ltd.

1. INTRODUCTION

The development of piezoelectric composite materials offers great potential for use in advanced aerospace structural applications. By taking advantage of the direct and converse piezoelectric effects, piezoelectric composite structures can combine the traditional performance advantages of composite laminates along with the inherent capability of piezoelectric materials to adapt to their current environment. Extensive development of analytical methods for modeling the isothermal behavior of piezoelectric composite structures has been reported. The initial application of piezoelectric materials as actuators involved the vibration control of beams [Bailey and Hubbard (1985); Crawley and de Luis (1987)] and led to the development of simplified models for beams. Advances in theoretical models led to both a piezoelectric plate theory [Lee (1990); Wang and Rogers (1991)] and a piezoelectric thin shell theory [Tzou and Gadre (1989)], based on the assumptions of classical plate and shell theory, respectively. Subsequent developments led to a variety of finite element formulations for beam [Robbins and Reddy (1991); Shieh (1994)], plate [Chandrashekhara and Agarwal (1993); Hwang and Park (1993)], shell [Lammering (1991); Tzou and Ye (1994a)], and solid [Allik and Hughes (1970); Tzou and Tseng (1990); Ha *et al.* (1992)] elements.

Additional approaches have been reported on refined piezoelectric laminate theories which overcome the limitations of classical or other "single-layer" laminate theories [Reddy (1987, 1993)]. These approaches, called discrete layer theories, provide a generalization of both the classical and higher order theories, and allow separate displacement fields to be assumed in each layer of the laminate. A discrete layer beam theory for analyzing piezoelectric beams was first reported by Robbins and Reddy (1991) using an induced strain approach to approximate the piezoelectric effect. Heyliger *et al.* (1994) and Saravanos and Heyliger (1995, 1996) subsequently presented discrete layer beam and plate theories

† Resident Senior Research Associate at NASA Lewis Research Center.

explicitly accounting for the coupled equations of piezoelectricity, which have led to generalized multi-field finite element formulations.

All of the previously described works neglect the implication of thermal effects on both the active and sensory response of piezoelectric structures, even though an area where piezoelectric materials may provide dramatic advantages is in the development of smart thermal structures with the capability to sense and actively compensate for thermally induced deformations. Thermal loads will typically affect the response of smart piezoelectric laminates with four distinct physical mechanisms: (1) induction of thermal strains due to coefficient of thermal expansion mismatch between the various composite plies and piezoelectric layers, (2) pyroelectric effects on the electric displacement of the piezoelectric material, (3) changes in the piezoelectric and dielectric properties of the piezoelectric materials, and (4) changes in the elastic properties of the composite and piezoelectric materials. Only limited research has been reported in this area. Two-dimensional thermopiezoelectric equations for plates was formulated by Mindlin (1974). A thermopiezoelectric laminate plate theory and a thin shell theory, based on classical assumptions, were reported by Tauchert (1992) and Tzou and Howard (1994), respectively. Subsequent developments in thermopiezoelectric finite elements include a beam element by Rao and Sunar (1993), a shell element using induced strain approximations for the electric and thermal effects by Chandrashekhara and Kolli (1995), a solid element using an induced thermal strain approach by Ha *et al.* (1992), and a thin solid element by Tzou and Ye (1994b). Many of these previous approaches utilize simplified laminate assumptions and neglect the coupling effects existing in thermopiezoelectric laminates. To remedy these limitations, generalized discrete layer approaches for smart thermopiezoelectric beam structures were reported by Lee and Saravanos (1995, 1996).

This paper presents generalized discrete layer mechanics for the analysis of smart thermopiezoelectric plate structures, and addresses the problem of active thermal distortion management with smart piezoelectric plates. The mechanics accounts for the coupled mechanical, electrical, and thermal response of piezoelectric laminates at the material level through the thermopiezoelectric constitutive equations. The displacements, electric potential and temperature are assumed to be layerwise (piecewise continuous) fields through the laminate thickness. This layerwise generalization provides the capability to capture the locally induced piezoelectric and thermal effects, which leads to increased accuracy in predicting the thermal response of piezoelectric composite plates (especially for thick laminates and laminates with strong thermal, piezoelectric and elastic inhomogeneities through-the-thickness). A corresponding finite element formulation is presented using the layerwise laminate theory and a 4-noded plate element is developed. Numerical studies demonstrate the capability to actively manage thermally induced twisting and bending deformations in piezoelectric symmetric and antisymmetric composite plates subjected to thermal gradients, as well as examining the corresponding voltage response of piezoelectric sensors and the resulting intralaminar and interlaminar stresses in active thermopiezoelectric plates.

2. GOVERNING MATERIAL EQUATIONS

This section outlines the governing equations for thermopiezoelectric materials. The mechanical response is represented by the stress-equilibrium equation,

$$\rho \ddot{u}_i = \sigma_{ij,j} + f_i, \quad i,j = 1,2,3 \tag{1}$$

where ρ, u_i, σ_{ij}, f_i are the density, displacement, stress, and body force per unit volume, respectively. The electrical response is governed by Maxwell's equation for the conservation of electric displacements D_i,

$$D_{i,i} = 0, \quad i = 1,2,3. \tag{2}$$

The constitutive equations for a thermopiezoelectric material [Nye (1964)] employing standard contracted notation are

$$S_\alpha = s^{E,T}_{\alpha\beta}(T)\sigma_\beta + d^T_{\alpha m}(T)E_m + \alpha^{E,\sigma}_\alpha(T)\theta \tag{3}$$

$$D_m = d^T_{m\alpha}(T)\sigma_\alpha + \varepsilon^{\sigma,T}_{mk}(T)E_k + p^{E,\sigma}_m(T)\theta \tag{4}$$

or in semi-inverted form

$$\sigma_\alpha = C^{E,T}_{\alpha\beta}(T)S_\beta - e^T_{\alpha m}(T)E_m - \lambda^{E,S}_\alpha(T)\theta \tag{5}$$

$$D_m = e^T_{m\alpha}(T)S_\alpha + \varepsilon^{S,T}_{mk}(T)E_k + p^{E,S}_m(T)\theta \tag{6}$$

where $\alpha, \beta = 1, \ldots, 6$; and $k, m = 1, 2, 3$; S_α represents the strain tensor; E_m the electric field vector, $\theta = \Delta T = T - T_o$ is the temperature difference from the current temperature T and the stress free reference temperature T_o; $C_{\alpha\beta}$ and $s_{\alpha\beta}$ are the elastic stiffness and compliance tensors; $d_{\alpha m}$ and $e_{\alpha m}$ are the different forms of the piezoelectric tensor; ε_{mk} is the electric permittivity tensor; α_α and λ_α are the different forms of the coefficient of thermal expansion; p_m is the pyroelectric constant; superscripts E, σ, S, and T, represent constant voltage, stress, strain, and temperature conditions, respectively. The matrices in eqs (3–4) and (5–6) are related as follows,

$$\begin{aligned}
e^T_{\alpha m}(T) &= C^{E,T}_{\alpha\beta}(T)d^T_{\beta m}(T)E_m \\
\lambda^{E,S}_\alpha(T) &= C^{E,T}_{\alpha\beta}(T)\alpha^{E,\sigma}_\beta(T) \\
\varepsilon^{S,T}_{mk}(T) &= \varepsilon^{\sigma,T}_{mk}(T) - d^T_{m\alpha}(T)e^T_{\alpha k}(T) \\
p^{E,S}_m(T) &= p^{\sigma,T}_m(T) - d^T_{m\alpha}(T)\lambda^{E,\sigma}_\alpha(T).
\end{aligned} \tag{7}$$

The small deformation strain-displacement relations are

$$S_{ij} = \frac{1}{2}(u_{i,j} + u_{j,i}) \tag{8}$$

and the electric field vector is related to the electric potential ϕ by

$$E_i = -\phi_{,i}. \tag{9}$$

Through use of the divergence theorem and neglecting body forces, eqs (1) and (2) can be expressed in an equivalent variational form as

$$\int_V (\rho\ddot{u}_i\delta u_i + \sigma_{ij}\delta S_{ij} - D_i\delta E_i)\mathrm{d}V = \int_\Gamma t_i\delta u_i\mathrm{d}\Gamma + \int_{\Gamma_p} q\delta\phi\mathrm{d}\Gamma \tag{10}$$

where t_i are the surface tractions applied on the bounding surface Γ; q is the electrical charge applied on the surface Γ_p of the piezoelectric material; and V represents the whole volume including both composite and piezoelectric materials.

3. DISCRETE LAYER LAMINATE THEORY

A discrete layer laminate theory for thermopiezoelectric composite plates is formulated by introducing the following piecewise continuous approximations for the state variables

$$u(x, y, z, t) = \sum_{j=1}^{N} u^j(x, y, t)\psi^j(z) \tag{11}$$

$$v(x, y, z, t) = \sum_{j=1}^{N} v^j(x, y, t)\psi^j(z) \tag{12}$$

$$w(x, y, z, t) = w^o(x, y, t) \tag{13}$$

$$\phi(x, y, z, t) = \sum_{j=1}^{N} \phi^j(x, y, t)\psi^j(z) \tag{14}$$

$$\theta(z, t) = \sum_{j=1}^{N} \theta^j(t)\psi^j(z) \tag{15}$$

where u^j, v^j, w^o, ϕ^j and θ^j are the generalized laminate state variables, $j = 1, \ldots, N$; and ψ^j are interpolation functions which are currently represented using linear Lagrangian interpolation functions, although in general any order of interpolation functions can be used. By substituting eqs (5)–(9) and (11)–(15) into eqn (10) and integrating through-the-thickness, the following generalized variational form is obtained.

$$\begin{aligned}
&\sum_{k=1}^{N}\sum_{m=1}^{N}\int_A (P_{11}^{km}\ddot{u}^m\delta u^k + P_{22}^{km}\ddot{v}^m\delta v^k)\mathrm{d}A + \int_A P_{33}\ddot{w}^o\delta w^o\mathrm{d}A \\
&\sum_{k=1}^{N}\sum_{m=1}^{N}\int_A \{A_{11}^{km}u_{,x}^m\delta u_{,x}^k + A_{12}^{km}(u_{,x}^m\delta v_{,y}^k + v_{,y}^m\delta u_{,x}^k) \\
&+ A_{16}^{km}(u_{,x}^m\delta u_{,y}^k + u_{,y}^m\delta u_{,x}^k + u_{,x}^m\delta v_{,x}^k + v_{,x}^m\delta u_{,x}^k) + A_{22}^{km}v_{,y}^m\delta v_{,y}^k \\
&+ A_{26}^{km}(u_{,y}^m\delta v_{,y}^k + v_{,y}^m\delta u_{,y}^k + v_{,x}^m\delta v_{,y}^k + v_{,y}^m\delta v_{,x}^k) \\
&+ A_{66}^{km}(u_{,y}^m\delta u_{,y}^k + u_{,y}^m\delta v_{,x}^k + v_{,x}^m\delta v_{,x}^k + v_{,x}^m\delta u_{,y}^k)\}\mathrm{d}A \\
&+ \sum_{m=1}^{N}\int_A \{B_{44}^m(v^m\delta w_{,y}^0 + w_{,y}^0\delta v^m) + B_{55}^m(u^m\delta w_{,x}^0 + w_{,x}^0\delta u^m) \\
&+ B_{45}^m(u^m\delta w_{,y}^o + v^m\delta w_{,x}^o + w_{,x}\delta v^m + w_{,y}^o\delta u^m)\}\mathrm{d}A \\
&+ \int_A \{\overline{C_{44}}w_{,y}^o\delta w_{,y}^o + \overline{C_{45}}(w_{,x}^o\delta w_{,y}^o + w_{,y}^o\delta w_{,x}^o) + \overline{C_{55}}w_{,x}^o\delta w_{,x}^o\}\mathrm{d}A \\
&\sum_{k=1}^{N}\sum_{m=1}^{N}\int_A \{D_{44}^{km}v^m\delta v^k + D_{45}^{km}(u^m\delta v^k + v^m\delta u^k) + D_{55}^{km}u^m\delta u^k \\
&+ E_{31}^{km}u_{,x}^m\delta\phi^k + E_{32}^{km}v_{,y}^m\delta\phi^k + E_{36}^{km}(u_{,y}^m\delta\phi^k + v_{,x}^m\delta\phi^k) \\
&+ \overline{E_{31}^{km}}\phi^m\delta u_{,x}^k + \overline{E_{32}^{km}}\phi^m\delta v_{,y}^k + \overline{E_{36}^{km}}(\phi^m\delta u_{,y}^k + \phi^m\delta v_{,x}^k) \\
&- G_{11}^{km}\phi_{,x}^m\delta\phi_{,x}^k - G_{22}^{km}\phi_{,y}^m\delta\phi_{,y}^k - G_{33}^{km}\phi^m\delta\phi^k\}\mathrm{d}A \\
&\sum_{m=1}^{N}\int_A \{-f_{th_1}^m\delta u_{,x}^m - f_{th_2}^m\delta v_{,y}^m + q_{th_1}^m\delta\phi_{,x}^m + q_{th_2}^m\delta\phi_{,y}^m + q_{th_3}^m\delta\phi^m\}\mathrm{d}A \\
&= \int_\Gamma t_i\delta u_i\mathrm{d}\Gamma + \int_{\Gamma_p} q\delta\phi\mathrm{d}T
\end{aligned} \tag{16}$$

in which the dependence of the z-coordinate has been separated into the generalized laminate matrices. The density matrix $[P]$, the stiffness matrices $[A]$, $[B]$, $[C]$, $[D]$, the

piezoelectric matrix [E], and the dielectric permittivity matrix [G] have been presented previously in a general form by Heyliger *et al.* (1994). The newly derived thermal force matrices [f_{th}] and [q_{th}] are

$$f^k_{th_i} = \sum_{i=1}^{L} \int_x \lambda_i \psi_j \theta_j \psi^k(z) \mathrm{d}z \tag{17}$$

$$q^k_{th_i} = \sum_{i=1}^{L} \int_x p_i \psi_j \theta_j \psi^k(z) \mathrm{d}z \tag{18}$$

for $i = 1$ and 2, while

$$q^k_{th_3} = \sum_{i=1}^{L} \int_x p_3 \psi_j \theta_j \frac{\partial \psi^k(z)}{\partial z} \mathrm{d}z \tag{19}$$

where L represents the number of piezoelectric layers and composite plies.

4. FINITE ELEMENT FORMULATION

The finite element formulation for a composite piezoelectric plate is obtained by incorporating additional local in-plane approximations to the generalized state variables introduced by eqns (11)–(14),

$$\langle u^j(x,y,t)\,;\, v^j(x,y,t)\,;\, w^o(x,y,t)\,;\, \phi^j(x,y,t)\rangle = \sum_{i=1}^{M} \langle U^{ji}(t)\,;\, V^{ji}(t)\,;\, W^{oi}(t)\,;\, \phi^{ji}(t)\rangle R^i(x,y) \tag{20}$$

where M is the number of in-plane functions R. Currently, R is represented using bilinear Lagrangian interpolation functions in the formulated 4-node element.

By combining eqn (20) with the variational statement eqn (16), the following finite element matrix formulation is obtained for the case of a constant through-the-thickness displacement plate

$$\begin{bmatrix} [M_{11}] & 0 & 0 & 0 \\ 0 & [M_{22}] & 0 & 0 \\ 0 & 0 & [M_{33}] & 0 \\ 0 & 0 & 0 & 0 \end{bmatrix} \begin{Bmatrix} \{\ddot{U}\} \\ \{\ddot{V}\} \\ \{\ddot{W}\} \\ \{\ddot{\Phi}\} \end{Bmatrix} + \begin{bmatrix} [K_{11}] & [K_{12}] & [K_{13}] & [K_{14}] \\ [K_{21}] & [K_{22}] & [K_{23}] & [K_{24}] \\ [K_{31}] & [K_{32}] & [K_{33}] & 0 \\ [K_{41}] & [K_{42}] & 0 & [K_{44}] \end{bmatrix} \begin{Bmatrix} \{U\} \\ \{V\} \\ \{W\} \\ \{\Phi\} \end{Bmatrix}$$
$$= \begin{Bmatrix} \{F_1\} \\ \{F_2\} \\ \{F_3\} \\ \{Q\} \end{Bmatrix} + \begin{Bmatrix} \{F_{1,th}\} \\ \{F_{2,th}\} \\ 0 \\ \{Q_{th}\} \end{Bmatrix} \tag{21}$$

where the elements of the submatrices above are calculated in accordance with the generalized discrete layer laminate matrices defined previously. The finite element sub-matrices for the mass [M], stiffness [K], and external force [F] and [Q] have been presented previously in a general form by Heyliger *et al.* (1994). The newly derived sub-matrices for the thermal force [F_{th}] and [Q_{th}] are

$$[F_{th}]_1^p = \int_A f_{th_1} \frac{\partial R^p(x,y)}{\partial x} \mathrm{d}A \tag{22}$$

$$[F_{th}]_2^p = \int_A f_{th_2} \frac{\partial R^p(x,y)}{\partial y} \mathrm{d}A \tag{23}$$

$$[Q_{th}]^p = \int_{A_p} \left\{ q_{th_1} \frac{\partial R^p}{\partial x} + q_{th_2} \frac{\partial R^p}{\partial y} + q_{th_3} R^p \right\} \mathrm{d}A. \tag{24}$$

The coupled finite element formulation can also be expressed in a compact form with the electric potential partitioned into active and sensory components such that

$$\begin{bmatrix} [M_{uu}] & 0 \\ 0 & 0 \end{bmatrix} \begin{Bmatrix} \{\ddot{U}\} \\ \{\ddot{\Phi}^s\} \end{Bmatrix} + \begin{bmatrix} [K_{uu}] & [K_{u\phi}^{ss}] \\ [K_{\phi u}^{ss}] & [K_{\phi\phi}^{ss}] \end{bmatrix} \begin{Bmatrix} \{U\} \\ \{\Phi^s\} \end{Bmatrix} = \begin{Bmatrix} \{F\} + \{F_{th}\} - [K_{u\phi}^{sa}]\{\Phi^a\} \\ \{Q^s\} + \{Q_{th}^s\} - [K_{\phi\phi}^{sa}]\{\Phi^a\} \end{Bmatrix} \tag{25}$$

where the superscripts s and a indicate the partitioned electric potential vectors in either sensory or active configurations, respectively. This form has the advantage of positioning the unknown variables (displacements and sensory electric potentials) in the left-hand terms, while the known quantities (mechanical loads, thermal loads, electric charges, and active voltages) are included in the right-hand terms. The partitioned finite element formulation of eqn (25) can be easily uncoupled into the following independent equations for the structural displacements

$$[M_{uu}]\{\ddot{U}\} + ([K_{uu}] - [K_{u\phi}^{ss}][K_{\phi\phi}^{ss}]^{-1}[K_{\phi u}^{ss}])\{U\} = \{F\} + \{F_{th}\} + ([K_{u\phi}^{ss}][K_{\phi\phi}^{ss}]^{-1}[K_{\phi\phi}^{sa}] - [K_{u\phi}^{sa}])\{\Phi^a\} \tag{26}$$

and the sensory electric potentials

$$\{\Phi^s\} = -[K_{\phi\phi}^{ss}]^{-1}([K_{\phi u}^{ss}]\{U\} + [K_{\phi\phi}^{sa}]\{\Phi^a\} - \{Q^s\} - \{Q_{th}^s\}). \tag{27}$$

5. APPLICATIONS

$[0/\pm 45]_s$ *graphite/epoxy plate with discrete piezoceramic patches*

This case study is a problem of active thermal distortion management, examined previously by Ha *et al.* (1992), of a 37.2 cm × 22.8 cm × 0.75 mm $[0/\pm 45]_s$ graphite/epoxy plate with fifteen 6.0 cm × 6.0 cm × 0.13 mm piezoceramic patches uniformly attached to each top and bottom surface. A thermal gradient (50°C on the top surface and −50°C on the bottom surface) is applied to the plate. Figure 1 illustrates the geometry and the finite element mesh of the plate. The plate is simply supported along the two edges parallel to the y-axis and is free on the two edges parallel to the x-axis. The material properties used for both the composite and piezoceramic materials are listed in Table 1. The objective was to apply increasing active voltages on both the top and bottom piezoceramic patches to minimize the out-of-plane deflection induced by the thermal gradient. Additional studies investigate the sensory response of the piezoceramic patches, as well as the development of local stresses in the plate with all piezoceramic patches operating as actuators.

Active thermal distortion control. The resulting bending deformation with 0 Volts applied on both surfaces of the piezoceramic patches is shown in Figure 2(a). Through application of increasing active voltages in the piezoceramic patches, the thermally induced deformation of the plate can be gradually eliminated. Figure 2(b) shows the reduction in out-of-plane deflection achieved by applying an active voltage of 70 V. The active voltage is applied on the outer surface of each piezoceramic patches, while the inner surface (i.e.,

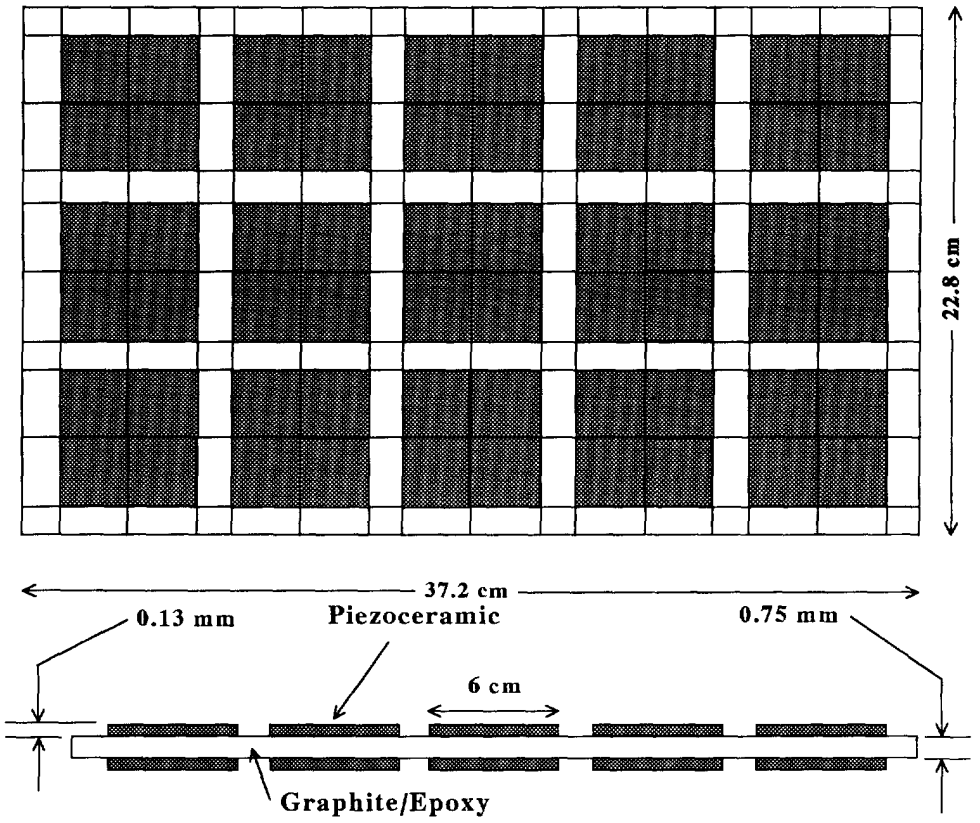

Fig. 1. Model of graphite/epoxy plate with attached piezoceramic patches. (a) Top view. (b) Front view.

the surface in contact with the plate) is grounded. Equal voltages are applied to both the upper and lower piezoceramic patches. A comparison of centerline deflections (along $y/b = 0.5$) predicted by Ha *et al.* (1992) and by the current formulation, along with the corresponding active voltages, is shown in Figure 3. In order to obtain the same reduction in centerline deflection as Ha *et al.*, slightly higher active voltages were applied using the current method (34 and 70 Volts, as compared to 31 and 61 Volts for Ha *et al.*). These differences between the two analyses are most likely due to the different formulations and elements used. Ha *et al.* used three-dimensional solid elements in their analysis, while the current method utilizes a layerwise plate theory and element which assumes a constant through-the-thickness displacement w. The present plate theory neglects certain material properties which Ha *et al.*'s analysis considers (specifically C_{13}, C_{23}, C_{33}, d_{24}, d_{33}, and α_{33}). Another difference is the explicit incorporation of thermal terms in the constitutive equations of the current formulation, which are neglected in Ha *et al.*'s analysis. Nevertheless, the overall good agreement shown in Figure 3 lends confidence to the accuracy of the current formulation.

Sensory voltages. Besides the fully active configurations previously studied (active potentials applied to all piezoceramic patches), other electric configurations yielding combinations of piezoceramic sensors and actuators are sometimes more desirable. The current formulation has the capability to explicitly predict sensory voltages. These sensory capabilities are demonstrated on an active/sensory configuration of the $[0/\pm 45]_s$ graphite/epoxy plate. The upper layer of piezoceramic patches is used as sensors, while the bottom layer of patches is maintained as actuators. Figure 4 shows the voltages that develop on the upper surface sensors upon combined application of a thermal gradient with an active voltage of 70 Volts on the lower piezoelectric patches. Generally, a reduction in the sensory voltage values was observed with increasing active voltages, which corresponds to the reduction in out-of-plane deflection, but additional contributions remain from local stresses

Table 1. Material properties of piezoceramic (PZT G1195N) and graphite/epoxy (T300/976) composite [Ha *et al.* (1992)]

	Piezoceramic	Graphite/epoxy
Elastic Moduli (GPa):		
E_{11}	63.0	150.0
E_{22}	63.0	9.0
E_{33}	63.0	9.0
Poisson's Ratio		
ν_{12}	0.3	0.3
ν_{23}	0.3	0.3
ν_{31}	0.3	0.3
Shear Moduli (GPa):		
G_{12}	24.2	7.10
G_{23}	24.2	2.50
G_{31}	24.2	7.10
Density (kg/m^3):		
ρ	7600	1600
Piezoelectric Charge Constant (pm/V):		
d_{14}	0.	0.
d_{15}	0.	0.
d_{24}	0.	0.
d_{25}	0.	0.
d_{31}	254.	0.
d_{32}	254.	0.
d_{36}	0.	0.
Electric Permittivity (nf/m):		
ε_{11}	15.3	0.
ε_{22}	15.3	0.
ε_{33}	15.0	0.
Thermal Expansion Coefficient (μm/m°C):		
α_{11}	0.9	1.1
α_{22}	0.9	25.2
Reference Temperature, T_o, (°C):	20	20

and pyroelectric effects. These measured sensory voltages will provide the inferred feedback essential for monitoring thermal distortions.

Local stresses. The development of high local stress fields in a thermopiezoelectric laminate from the mismatch in induced thermal and piezoelectric strains is also an area of primary concern, since it will affect the integrity of these structures. As stated previously, one strong advantage of the layerwise approach is the accurate calculation of intralaminar in-plane stresses and interlaminar shear stresses in piezoelectric composite laminates [Heyliger *et al.* (1994); Saravanos and Heyliger (1995, 1996)]. Consequently, this section presents the stress fields for the active $[0/\pm 45]_s$ graphite/epoxy plate problem. In these studies, a continuous piezoceramic layer is used instead of many distributed piezoceramic patches to eliminate the need for a highly refined mesh. The stresses are non-dimensionalized using an equivalent laminate moduli defined as

$$\langle E_{Lij}, G_{Lij} \rangle = \frac{1}{h} \int_0^h \langle E_{ij}, G_{ij} \rangle \mathrm{d}z.$$

Figures 5(a–b) show the variation of normal stress (σ_{xx}) and out-of-plane shear stress (σ_{xz}) through-the-thickness under different applied voltages. The normal stress in Fig. 5(a) increases as higher active voltages are applied reflecting the increase in piezoelectric strains,

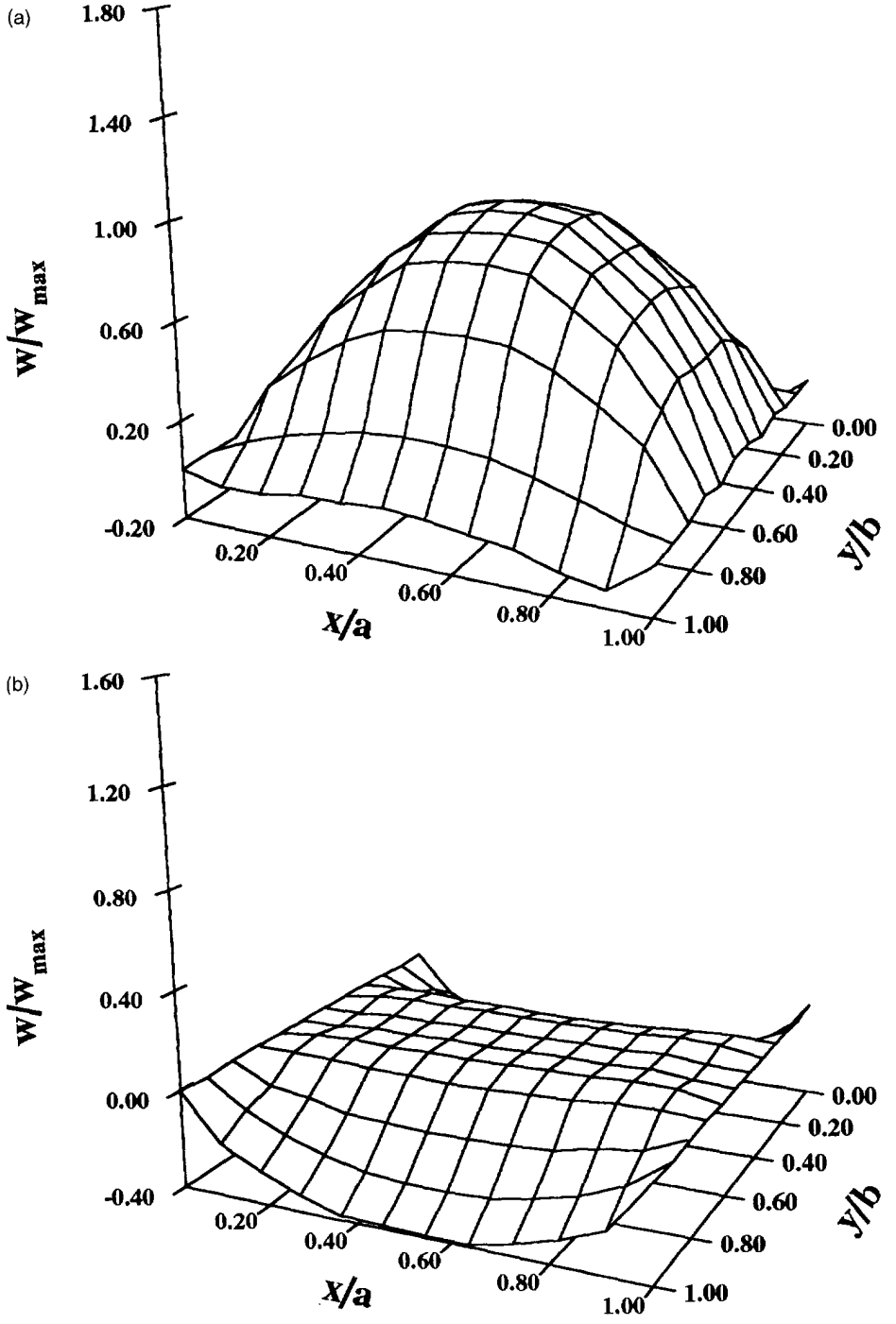

Fig. 2. Active compensation of thermal deformation of $[0/\pm 45]_s$ plate subject to 100°C gradient. (a) 0 Volts applied on upper and lower piezoceramic patches. (b) 70 Volts applied on upper and lower piezoceramic patches.

which indicates that one potential tradeoff for minimizing thermal distortions would be increased normal stress. In contrast, the out-of-plane shear stress (σ_{xz}) in Fig. 5(b) decreases with increasing active voltages. The normal stress σ_{xx} can also be separated into individual components as shown in Fig. 6 for the 70 V case. The three components correspond to the three terms found on the right hand side of eqn (5) and represent the individual stresses which are induced from the elastic, piezoelectric, and thermal effects.

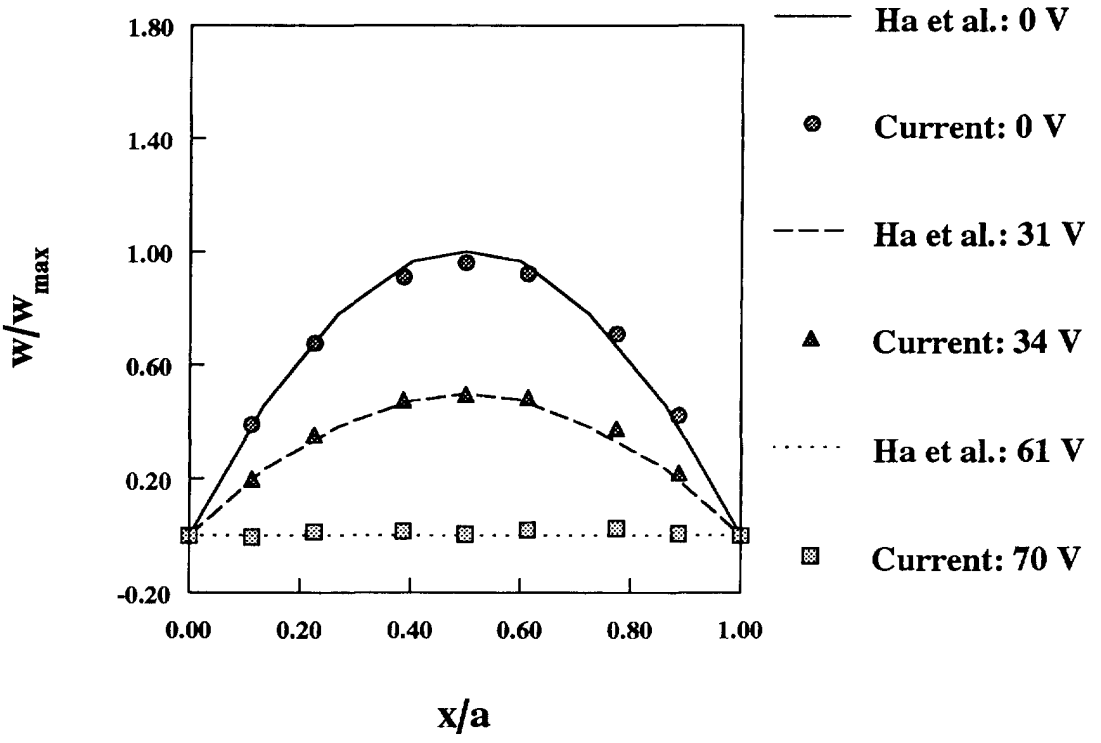

Fig. 3. Centerline ($y/b = 0.5$) deflections of $[0/\pm 45]_s$ plate.

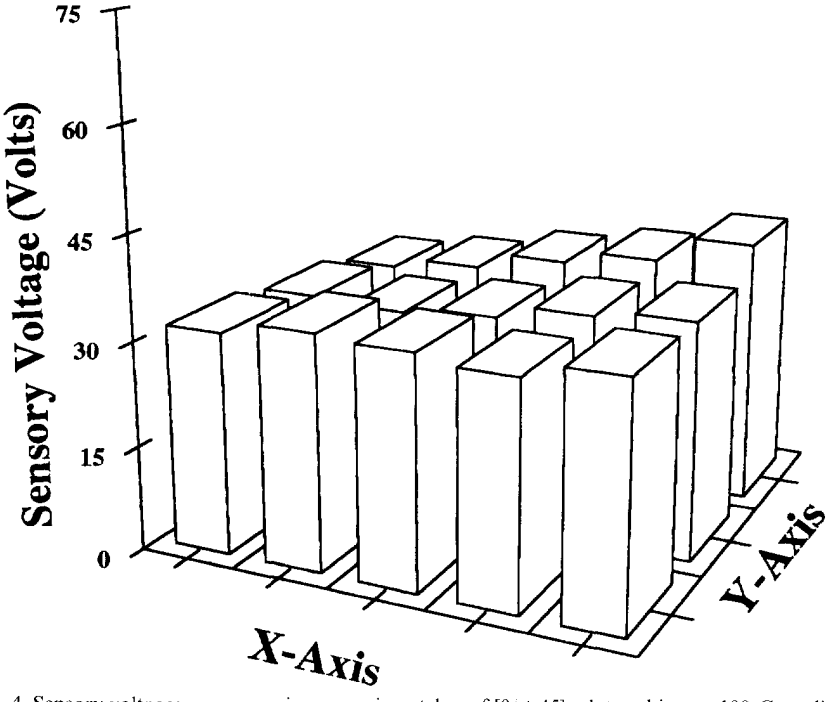

Fig. 4. Sensory voltages on upper piezoceramic patches of $[0/\pm 45]_s$ plate subject to 100 C gradient with 70 Volts applied on lower piezoceramic patches.

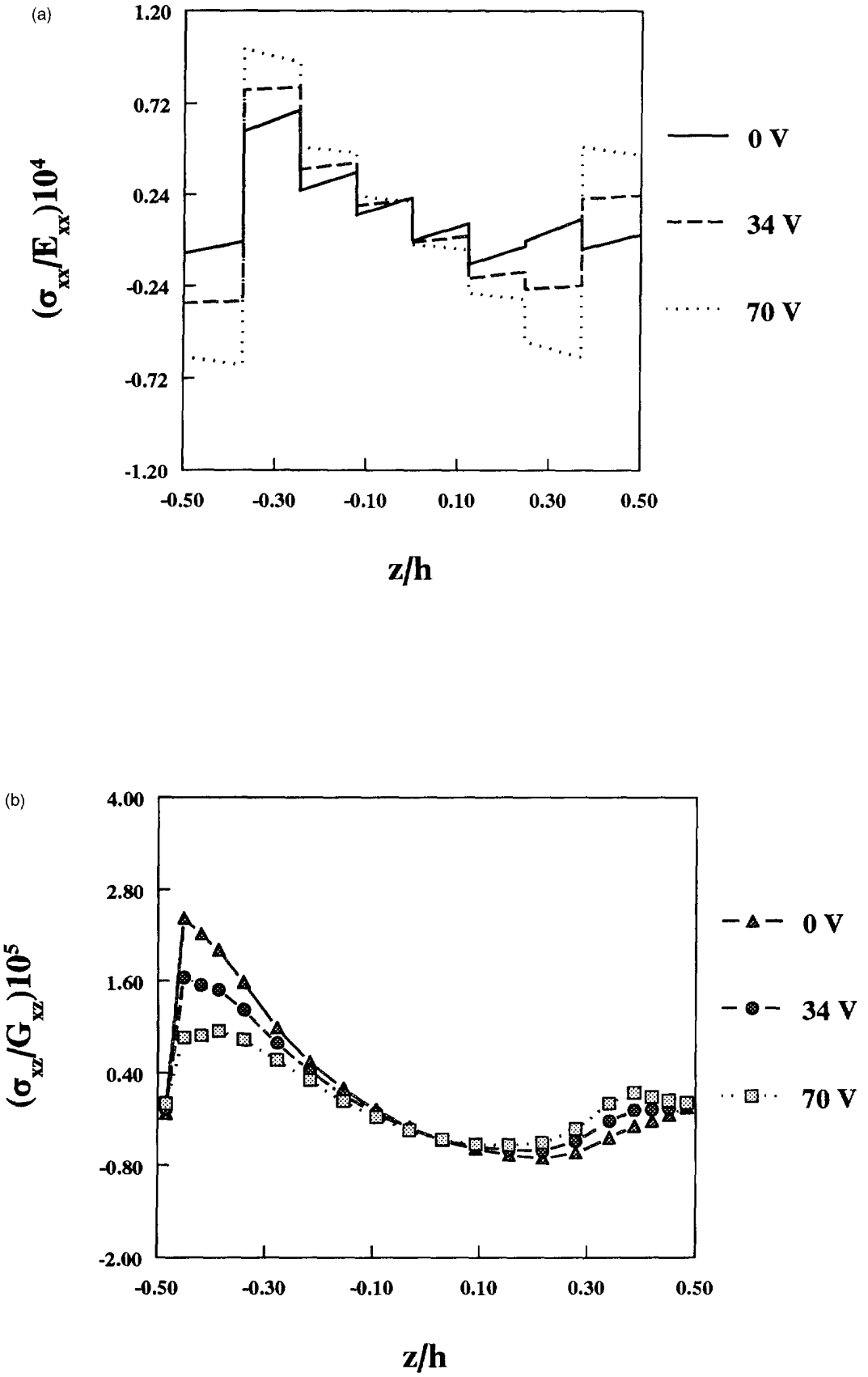

Fig. 5. Through-the-thickness stresses in $[0/\pm 45]_s$ plate subject to 100°C gradient and applied voltages on upper and lower piezoceramic patches. (a) σ_{xx} at $(x/a = 0.5, y/b = 0.4)$. (b) σ_{xz} at $(x/a = 0.9, y/b = 0.4)$.

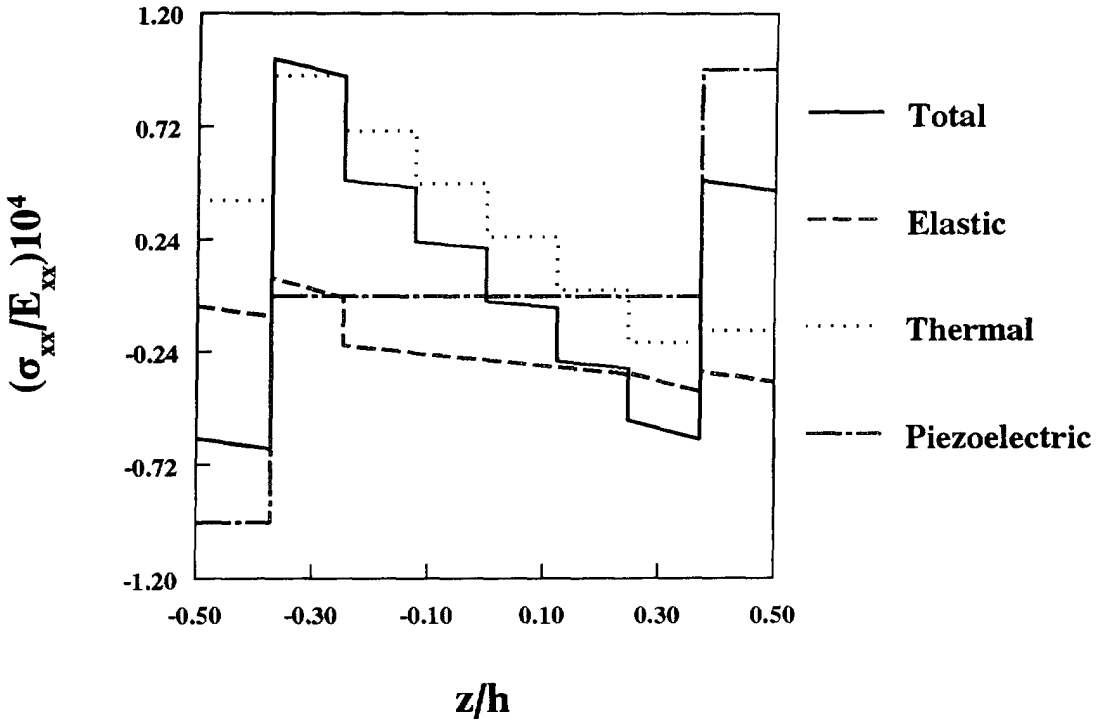

Fig. 6. Elastic, thermal, and piezoelectric components of σ_{xx} in $[0/\pm 45]_s$ plate subject to 100°C gradient and 70 Volts applied on upper and lower piezoceramic patches.

$[45_3/-45_3]$ *graphite/epoxy plate with discrete piezoceramic patches*

A numerical study was also conducted on a cantilevered $[45_3/-45_3]$ antisymmetric graphite/epoxy plate with attached piezoceramic patches. The plate has the same geometry and material properties used in the previous section and is clamped along the $x = 0$ edge, while the other three edges remain free. A thermal gradient (15°C on the top surface and −15°C on the bottom surface) is applied to the plate with 0 Volts applied on both surfaces of the piezoceramic patches. The objective of this study is to minimize, both individually and in combination, the thermally induced bending and twisting deformations through application of active voltages.

Active thermal distortion control. Application of a 30°C thermal gradient, with all piezoceramic patches grounded, results in the combined thermal bending and twisting deformation shown in Fig. 7(a). Through application of active voltages of varying polarities in the piezoceramic patches, the bending and twisting deformations can be inhibited either individually or in combination. As demonstrated in the previous problem, the bending deformation can be managed through application of voltages which have the opposite polarity. By applying 40 V to both the top and bottom layers of piezoceramic patches, the bending deformation can be eliminated as shown in Fig. 7(b). The twisting deformation remains unaffected and is now more apparent due to the removal of thermal bending. In a similar manner, the twisting deformation of the plate can be eliminated, without affecting the bending behavior as shown in Fig. 7(c). This requires the application of voltages with the same polarities, specifically 145 V is applied to the top layer of piezoceramic patches, while −145 V is applied to the bottom layer of piezoceramic patches. Finally, in order to inhibit both the bending and twisting deformations simultaneously, the previous voltages are superposed. Thus, by applying 185 V on the upper and −105 V on the lower piezoceramic patches, all deformations in the plate can be compensated, as shown in Fig. 7(d). These results demonstrate the potential of piezoelectric structures to selectively manage desired thermal distortions.

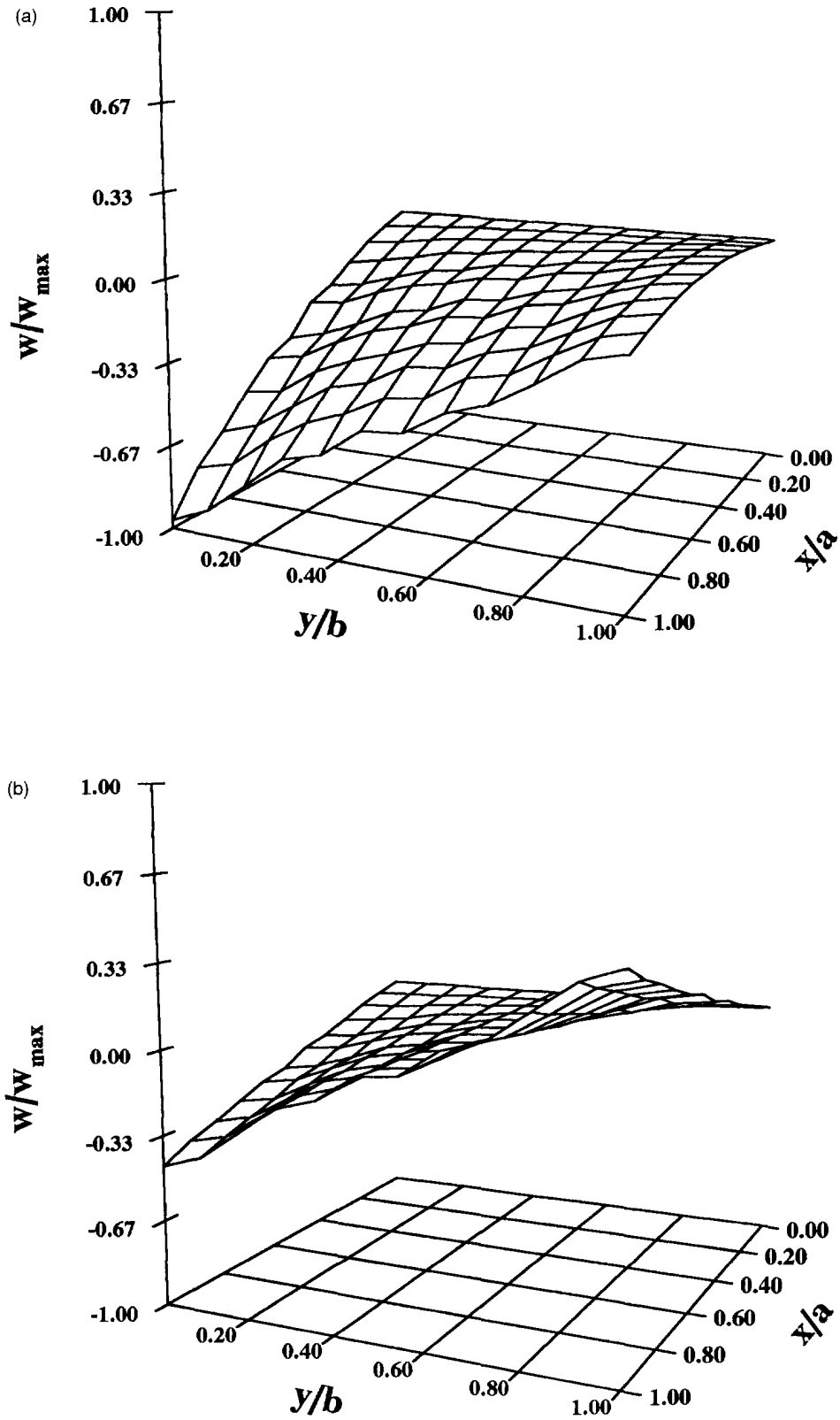

Fig. 7. Active compensation of thermal bending and twisting deformation of $[45_3/-45_3]$ plate subject to 30°C gradient. (a) Initial thermal deformation: 0 Volts applied on upper and lower piezoceramic patches. (b) Active compensation of thermal bending: 40 Volts applied on upper and lower piezoceramic patches. (c) Active compensation of thermal twisting: 145 Volts applied on upper and −145 Volts on lower piezoceramic patches. (d) Complete compensation of thermal deformation: 185 Volts applied on upper and −105 Volts on lower piezoceramic patches. (*Continued overleaf.*)

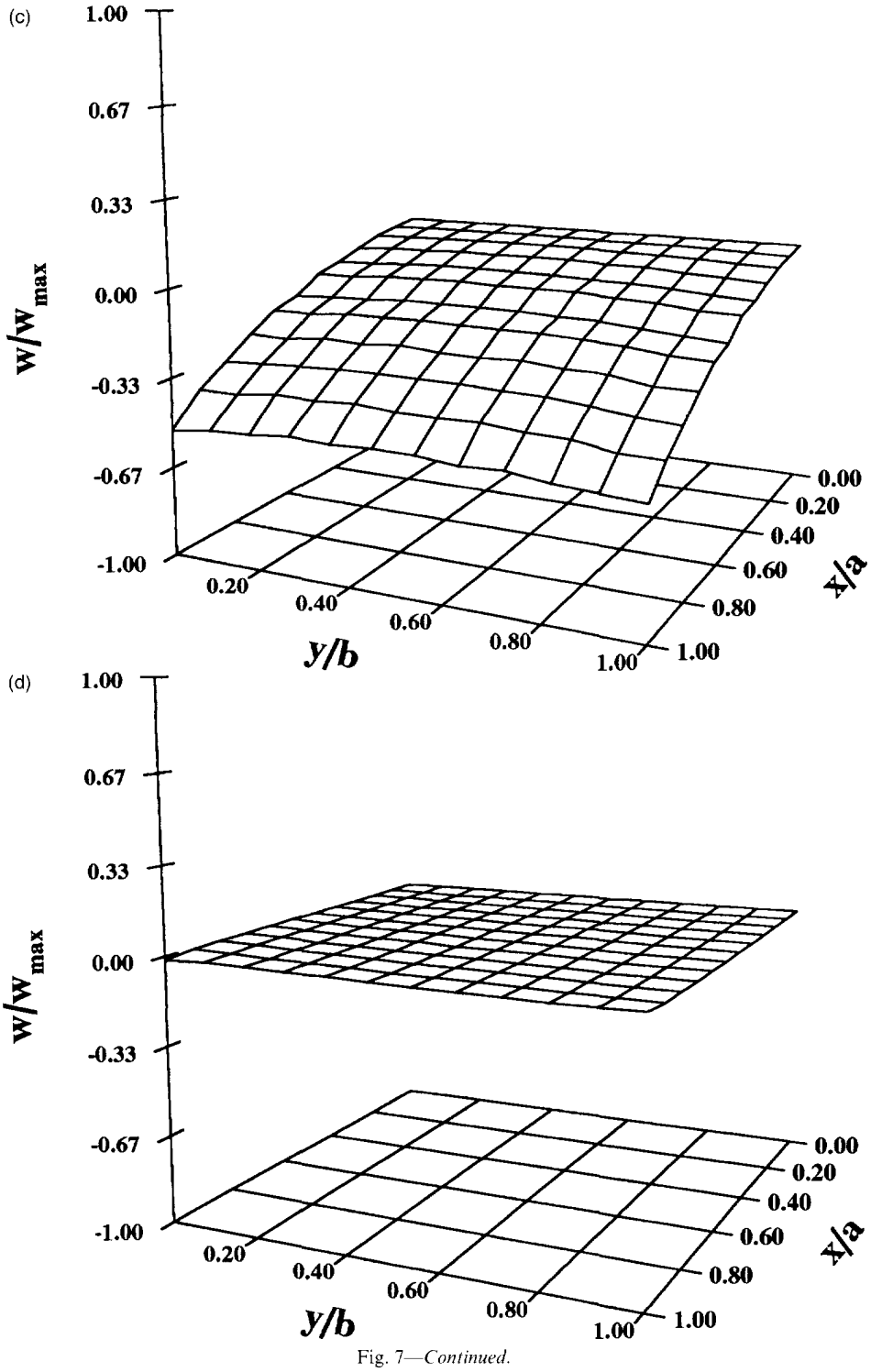

Fig. 7—*Continued.*

Local stresses. This section demonstrates the advantage of the layerwise approach in calculating interlaminar shear stresses by examining the stress fields for the $[45_3/-45_3]$ graphite/epoxy plate. In general, classical plate theory provides accurate in-plane results for low thickness laminates. However, the classical theory neglects interlaminar shear stresses and becomes inaccurate in the analysis of both thick laminates and laminates with strong inhomogeneities. In order to demonstrate the advantages of the discrete layer theories, three different laminate thicknesses are examined corresponding to a thin plate

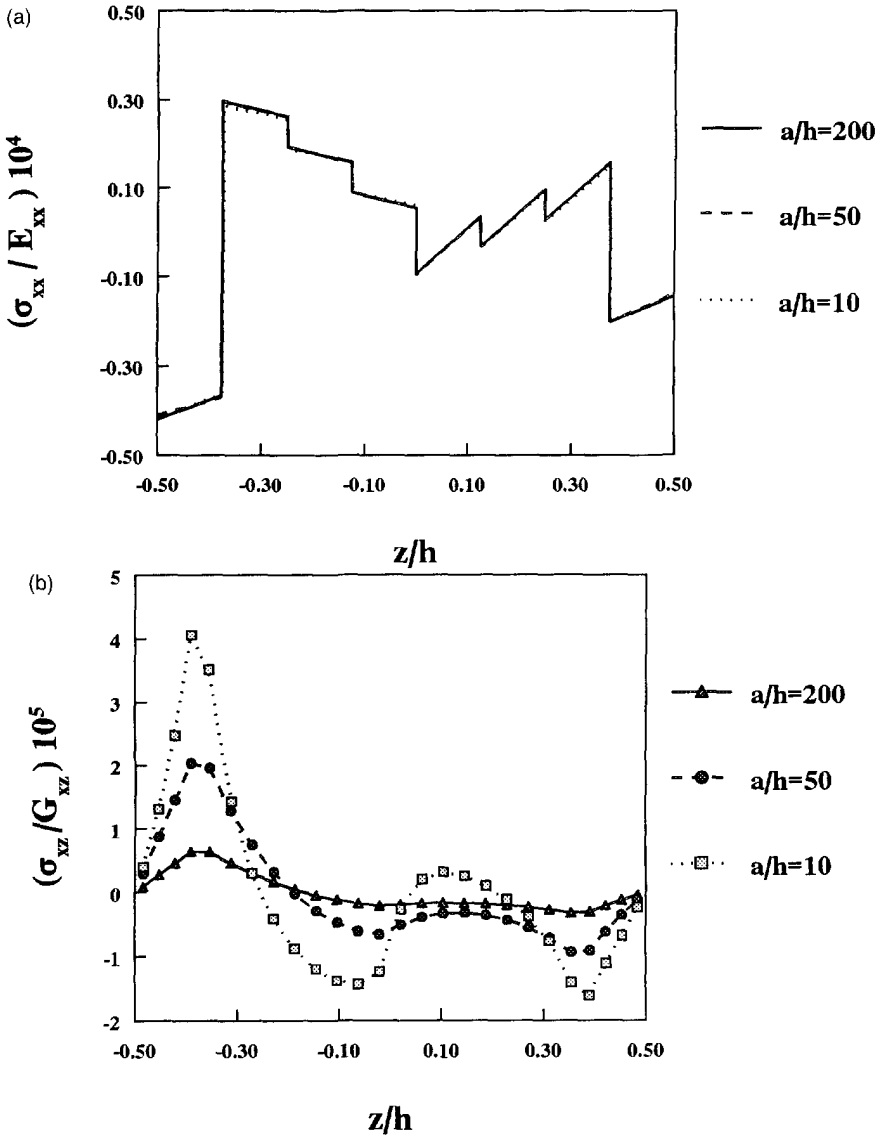

Fig. 8. Through-the-thickness stress in $[45_3/-45_3]$ plate subject to 30°C gradient and 0 Volts applied on upper and lower piezoceramic patches. (a) σ_{xx} at $(x/a = 0.5, y/b = 0.4)$. (b) σ_{xz} at $(x/a = 0.9, y/b = 0.4)$.

$(a/h = 200)$, a plate of intermediate thickness $(a/h = 50)$, and a thick plate $(a/h = 10)$ for the case in which a 30°C thermal gradient is applied with all piezoceramic patches grounded. As before, a continuous piezoceramic layer is used instead of many distributed piezoceramic patches to eliminate the need for a highly refined mesh in this study. Figure 8(a) shows the through-the-thickness variation of normal stress (σ_{xx}) near the center of the plate, while Fig. 8(b) shows the out-of-plane shear stress (σ_{xz}) near the free end for different aspect ratios. Figure 8(a) shows that the normal stress (away from the free end) remains relatively insensitive to changes in the aspect ratio. In contrast, as shown in Fig. 8(b), the magnitude of the out-of-plane shear stress near the free end increases as the laminate thickness increases. Since both the shear stress and thickness effect are not captured by the classical theory, this example helps to demonstrate the importance of the present layerwise approach in the accurate prediction of critical stresses in smart thermo-piezoelectric composite plates.

6. SUMMARY

Layerwise laminate and structural mechanics were described to model the coupled mechanical, electrical, and thermal behavior of smart piezoelectric composite laminates

and plate structures. A finite element formulation and a bilinear 4-noded plate element were developed and encoded into prototype software, thus establishing a significant analytical and computational capability for analyzing the response of thermally stable smart piezoceramic plate structures operating in thermal environments.

The accuracy of the formulation was compared with previously published analytical results. Numerical studies were performed on symmetric $[0/\pm 45]_s$ and antisymmetric $[45_3/-45_3]$ composite plates subject to thermal gradient with discrete piezoceramic patches attached on both surfaces, which demonstrated the capability to actively manage thermally induced bending and twisting deformations. The corresponding electric voltages developed at distributed piezoelectric sensors were also calculated. Finally, the severe stress fields through-the-thickness of the composite plates were predicted and the contributions of the thermal and piezoelectric components quantified. The numerical studies have indicated the significance of thermal effects on the performance of piezoelectric structures in extreme temperature environments and demonstrated the capabilities of the mechanics to accurately model such behavior.

REFERENCES

Allik, H. and Hughes, T. J. R. (1970). Finite element method for piezoelectric vibration. *International Journal of Numerical Methods in Engineering* **2**, 151–157.

Bailey, T. and Hubbard, J. E. (1985). Distributed piezoelectric-polymer active vibration control of a cantilever beam. *Journal of Guidance*, **8**, 605–611.

Chandrashekhara, K. and Agarwal, A. N. (1993). Active vibration control of laminated composite plates using piezoelectric devices: a finite element approach. *Journal of Intelligent Materials, Systems and Structures* **4**, 496–508.

Chandrashekhara, K. and Kolli, M. (1995). Thermally induced vibration of adaptive doubly curved composite shells with piezoelectric devices. In *Proc. 36th Structures, Structural Dynamics, and Materials Conference*, New Orleans, LA, 10–13 April 1995, pp. 1628–1636.

Crawley, E. F. and de Luis, J. (1987). Use of piezoelectric actuators as elements of intelligent structures. *AIAA Journal* **25**, 1373–1385.

Ha, S. K., Keilers, C. and Chang, F.-K. (1992). Finite element analysis of composite structures containing distributed piezoceramic sensors and actuators. *AIAA Journal* **30**, 772–780.

Heyliger, P. R., Ramirez, G. and Saravanos, D. A. (1994). Coupled discrete-layer finite elements for laminated piezoelectric plates. *Communications in Numerical Methods in Engineering* **10**, 971–981.

Hwang, W.-S. and Park, H. C. (1993). Finite element modeling of piezoelectric sensors and actuators. *AIAA Journal* **31**, 930–937.

Lammering, R. (1991). The application of a finite shell element for composites containing piezoelectric polymers in vibration control. *Computers & Structures* **41**, 1101–1109.

Lee, C. K. (1990). Theory of laminated piezoelectric plates for the design of distributed sensors/actuators. Part I: governing equations and reciprocal relationships. *Journal of the Acoustic Society of America* **87**, 1144–1158.

Lee, H.-J. and Saravanos, D. A. (1995). On the response of smart piezoelectric composite structures in thermal environments. In *Proc. 36th Structures, Structural Dynamics, and Materials Conf.*, New Orleans, LA, 10–13 April 1995, pp. 2876–2885.

Lee, H.-J. and Saravanos, D. A. (1996). Coupled layerwise analysis of thermopiezoelectric composite beams. *AIAA Journal* **34**, 1231–1237.

Mindlin, R. D. (1974). Equations of high frequency vibrations of thermopiezoelectric crystal plates. *International Journal of Solids and Structures* **10**, 625–632.

Nye, J. F. (1964). *Physical Properties of Crystals*. The Clarendon Press, Oxford.

Rao, S. S. and Sunar, M. (1993). Analysis of distributed thermopiezoelectric sensors and actuators in advanced intelligent structures. *AIAA Journal* **31**, 1280–1286.

Reddy, J. N. (1987). A generalization of two-dimensional theories of laminated composite plates. *Communications in Numerical Methods in Engineering* **3**, 173–180.

Reddy, J. N. (1993). An evaluation of equivalent single-layer and layerwise theories of composite laminates. *Computers & Structures* **25**, 21–35.

Robbins, D. H. and Reddy, J. N. (1991). Analysis of piezoelectrically actuated beams using a layer-wise displacement theory. *Computers & Structures* **41**, 265–279.

Saravanos, D. A. and Heyliger, P. R. (1995). Coupled layerwise analysis of composite beams with embedded piezoelectric sensors and actuators. *Journal of Intelligent Materials, Systems and Structures* **6**, 350–363.

Saravanos, D. A. and Heyliger, P. R. (1997). Layerwise mechanics and finite element for the dynamic analysis of piezoelectric composite plates. *International Journal of Solids and Structures* (in press).

Shieh, R. C. (1994). Governing equations and finite element methods for multiaxial piezoelectric beam sensors/actuators. *AIAA Journal* **32**, 1250–1258.

Tauchert, T. R. (1992). Piezothermoelastic behaviour of a laminated plate. *Journal of Thermal Stresses* **15**, 25–37.

Tzou, H. S. and Gadre M. (1989). Theoretical analysis of a multi-layered thin shell coupled with piezoelectric shell actuators for distributed vibration controls. *Journal of Sound and Vibration* **132**, 433–450.

Tzou, H. S. and Howard, R. V (1994). A piezothermoelastic thin shell theory applied to active structures. *Journal of Vibration and Acoustics* **116**, 295–302.

Tzou, H. S. and Tseng, C. I. (1990). Distributed piezoelectric sensor/actuator design for dynamic measurement/control of distributed parameter systems: a piezoelectric finite element approach. *Journal of Sound and Vibration* **138**, 17–34.

Tzou, H. S. and Ye, R. (1994a). Analysis of laminated piezoelectric shell systems with C^0 piezoelectric triangle finite elements. In *Proc. Adaptive Structures and Composite Materials: Analysis and Application*. ASME, Vol. AD-45, pp. 113–124.

Tzou, H. S. and Ye, R. (1994b). Piezothermoelasticity and precision control of piezoelectric systems: theroy and finite element analysis. *Journal of Vibration and Acoustics* **116**, 489–495.

Wang, B.-T. and Rogers, C. A. (1991). Laminate plate theory for spatially distributed induced strain actuators. *Journal of Computers and Materials* **25**, 433–452.